

A First-Principles Investigation of Phonon Softenings and Lattice Instabilities in the Shape-Memory System Ni₂MnGa

A. T. Zayak, and P. Entel

Institute of Physics, Gerhard-Mercator University, 47048, Duisburg, Germany

J. Enkovaara, A. Ayuela, and R. M. Nieminen

Laboratory of Physics, Helsinki University of Technology, 02015 Espoo, Finland

(Dated: October 29, 2018)

Ferromagnetic Ni₂MnGa has unique magnetoelastic properties. These are investigated by detailed computational studies of the phonon dispersion curves for the non-modulated cubic L₂₁ and tetragonal structures. For the L₂₁ structure, a complete softening of the transverse acoustic mode has been found around the wave vector $\mathbf{q} = [1/3, 1/3, 0](2\pi/a)$. The softening of this TA₂ phonon mode leads to the premartensitic modulated super-structure observed experimentally. Further phonon anomalies, related to other structural transformations in Ni₂MnGa, have also been found and examined. These anomalies appear to be due to the coupling of particular acoustic phonon modes and optical modes derived from Ni.

Displacive, diffusionless structural transformations of the martensitic type are known to occur in many metallic alloys. These transformations involve cooperative rather than diffusive displacements of atoms and are often associated with phonon anomalies in the parent phase and related precursor phenomena. It is a general challenge of the fundamental physics to explain driving forces of the martensitic transformations.

Since the discovery of a martensitic transformation in ferromagnetic Ni₂MnGa [1], this material has attracted strong interest [2]. This Heusler alloy is one of the very rare magnetic materials which undergo a martensitic transformation below the Curie temperature, whereby the combination of magnetic and structural features is responsible for its unique magnetomechanical properties. Shear deformations of more than 5 % have been obtained in magnetic fields [3, 4, 5]. These features together make Ni₂MnGa very efficient for magnetic-shape-memory (MSM) technology [6]. The MSM technology is based on the magnetic field induced redistribution of martensitic domains in the sample. From the technological point of view, Ni₂MnGa is much more promising than other materials being presently in commercial use, for example the well-known material Tb-Dy-Fe (Terfenol-D) which exhibits magnetostrictive strains of about 0.1 %. Design of new efficient MSM magneto-mechanical actuator devices is in progress [7]. Also the search for new materials with magnetic shape-memory effects is underway, even in antiferromagnets [8].

Despite the experimental and technological success, a microscopic theory is missing, which would be able to show how far the premartensitic phase transition will result from the coupling of soft phonon modes and homogeneous strains associated with the shear constant C' [9, 10]. A complete understanding requires the evaluation of the phonon spectrum. The aim of this letter is to present supercell phonon calculations for the L₂₁ and T structures (see Fig. 1 and Table I) using a state-of-the-

art first-principles method based on density-functional theory.

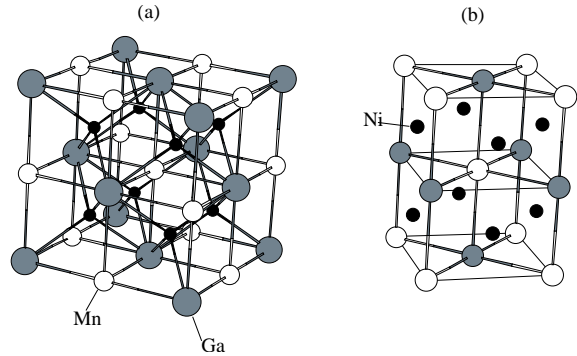


FIG. 1: (a) Simple cubic cell of Ni₂MnGa (Heusler L₂₁ structure); (b) tetragonal bct cell in the [110] direction. The equilibrium lattice parameter obtained is $a_{\text{cubic}} = 5.8067 \text{ \AA}$ and agrees with the experimental value [1]. The direction [010]_{orth} of the supercell corresponds to the direction [110]_{cubic} of the cubic structure. As the supercell consists of five tetragonal cells, the lattice parameters of the supercell are related to the lattice parameters of the cubic L₂₁ structure as follows: $a_{\text{orth}} = (1/\sqrt{2})a_{\text{cubic}}$, $b_{\text{orth}} = (5/\sqrt{2})a_{\text{cubic}}$, $c_{\text{orth}} = a_{\text{cubic}}$.

Ni₂MnGa is ferromagnetic at room temperature ($T_C \approx 380 \text{ K}$) and undergoes a two-step martensitic phase transformation. As a matter of fact, a number of different thermal and stress-induced martensitic structures have been observed in Ni₂MnGa [11]. Table I gives a summary of the structures found for Ni₂MnGa [1, 10, 11]. In the parent phase, several phonon anomalies can be observed with decreasing temperature. At the temperature $T \approx 260 \text{ K}$, a nearly complete softening of the $[1/3, 1/3, 0](2\pi/a)$ transverse acoustic TA₂ mode with polarization along [110] leads to a premartensitic phase transition, which has been evidenced by neutron scattering [10, 12, 13, 14], X-ray [15], electron microscopy [16], and ultrasonic measurements [17, 18] or a combina-

tion of the previous methods [19]. This structural transformation involves a commensurate periodic distortion of the parent phase with a propagation vector equal to that of the soft mode $\mathbf{q} = [1/3, 1/3, 0](2\pi/a)$ corresponding to six atomic planes or three lattice spacings. The precursor phenomena involves the magneto-elastic coupling as it has been described using Landau-type models [20]. These phenomenological models take as input very important lattice-dynamical properties. Thus, explicit calculation of the lattice dynamics is required since in transition metals, the d -electrons allow for many types of coupling, and several modes can be involved.

TABLE I: Structural parameters of the crystal structures of Ni-Mn-Ga alloys according to Ref. [11] and this work. They follow (from left to right) the order of possible appearance when lowering the temperature. There is a superimposed modulation specified by the notation nL , where n stands for the close commensurate number of bct cells in the [110] direction; their respective \mathbf{q} vectors are in units of $(2\pi/a)$. The so-called premartensitic transformation happens between the L2_1 and 3L structures.

Axes		Lattice parameters (Å)				
		L2_1	3L	5L	7L	T
a		5.824	5.824	5.90	6.12	6.44
b		5.824	5.824	5.90	5.78	5.52
c		5.824	5.824	5.54	5.54	5.52
Modulation	none	$\mathbf{q} \approx 0.33$	$\mathbf{q} \approx 0.43$?	?	none
Tetragonality		1	1	0.94	-	≈ 1.2

For the sake of simplicity, we present phonon calculations for the direction [110], which is the most interesting one as seen from the measurements for the acoustic modes [13]. We have used the direct method for the evaluation of the phonon dispersion curves [21, 22], whereby the Hellmann-Feynman forces are calculated with the Vienna *Ab-initio* Simulation Package (VASP) [23, 24] and the implemented projected augmented wave formalism (PAW) [25]. Within density-functional theory, the electronic exchange and correlation are treated by using the generalized gradient approximation (GGA). The $3d$ electrons of Ga have been included as valence states. The importance of using PAW for Ni_2MnGa instead of pseudopotentials has been pointed out earlier [26]. An orthorhombic supercell of 40 atoms formed by five tetragonal crystallographic unit cells, as seen in Fig. 1(b), has been used to calculate the phonon spectrum for the [110] direction [27]. The direct method implies that we calculate forces induced on all atoms of the supercell when a single atom is displaced from its equilibrium position. Displacement of the atoms in only one tetragonal unit cell along all directions allows one to derive the force constant matrix and the dynamical matrix. Diagonalization of the dynamical matrix then leads to a set of eigenvalues for the phonon frequencies and corresponding eigenvectors.

The calculations have been done by using an amplitude for the displacements of $u = 0.03 \text{ \AA}$. This value is sufficient to calculate the forces with required precision and to fulfill the conditions of the harmonic approximation.

Phonon dispersion curves calculated for Ni_2MnGa in the $[110]_{\text{cubic}}$ direction are shown in Fig. 2(a). The acoustic modes are qualitatively and quantitatively in very good agreement with experimental results obtained from inelastic neutron scattering [13]. For instance, following the acoustic branch, the values of the TA_2 branch at $\zeta = 1$, of the crossing between LA and TA_1 branch, and of the maximum of the LA branch are 2.33, 4.43 and 5.13 THz, in good agreement with the experimental ones, 2.67, 4.35 and 5.07 THz [13]. The initial slopes of the curves in the longitudinal ($v_L = 5.23 \times 10^5 \text{ m/s}$) and transverse ($v_{\text{TA}_1} = 3.35 \times 10^5 \text{ m/s}$; $v_{\text{TA}_2} = 1.02 \times 10^5 \text{ m/s}$) modes agree well with the sound velocities measured via the neutron scattering dispersion curves [13]. The slope of the phonon dispersion curves around the Γ point is positive, which is consistent with the stability around this phase.

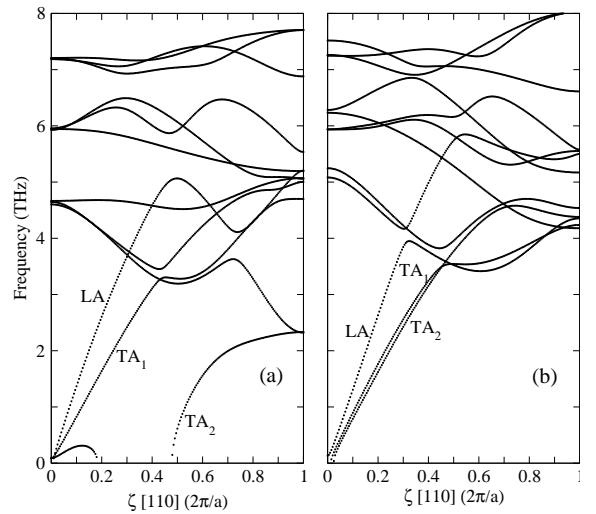


FIG. 2: Phonon dispersion curves for the cubic L2_1 structure (a) and the tetragonal T structure (b) of Ni_2MnGa . Here, the reduced wave vector coordinate ζ spans the fcc BZ from Γ to X .

We find a complete softening of the transverse acoustic TA_2 phonon mode between $\zeta = 0.2$ and $\zeta = 0.55$. This softening occurs around the wave vector coordinate $\zeta = 1/3$, which corresponds to the soft-mode phonon anomaly observed in the experimental studies [13]. We point out that the experimentally observed premartensitic transition is related to this soft mode.

The softening of the TA_2 mode means that the cubic L2_1 high-temperature structure is unstable at zero temperature with respect to a particular atomic displacement leading to the formation of a modulated premartensitic structure. The 3L structure can be modeled by a large

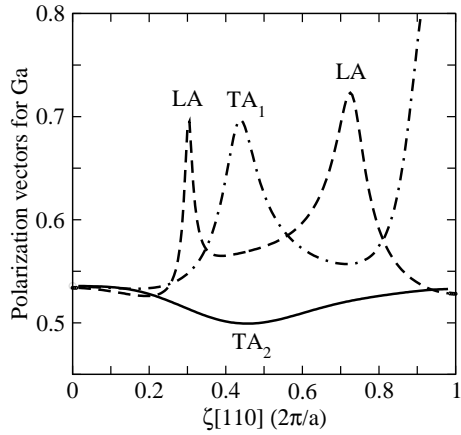


FIG. 3: Polarization vectors corresponding to the acoustic phonon modes of Ga. The peaks at $\zeta = 0.300$, $\zeta = 0.433$ and $\zeta = 0.715$ are due to the coupling to the optical modes of Ni.

supercell composed of three basic bct supercells in the [110] direction (see Fig. 4) [28]. The atoms of the input structure have a modulated amplitude with a maximum around 0.05 \AA where the Ni atoms are in opposite phase to the Mn and Ga atoms. Full relaxation of the three lattice parameters, a , b and c has been allowed. Also, lower magnetizations of 60-80 % of the full magnetization value for the whole supercell has been taken into account. In addition, two periods commensurate with the lattice were tested, but the structure with one period, as shown in Fig. 4, gives the minimum energy. The static displacements of the 3L modulated structure are shown in Fig. 4(b). The modulation of the atoms stays in phase which differs from the input data, but it is typical for an acoustic branch such as TA_2 . The amplitudes for all the atoms are nearly the same, although they differ slightly but not according to the atom masses. Rather, the order is according to the sequence of the optical phonons energies, where Ni has the lowest energy, optical modes of Ga are in the next energy windows, and Mn optical phonons are of the highest energy (see Fig. 2).

We have considered so far only the acoustic mode TA_2 , because this mode is responsible for the phase transformation $\text{L2}_1 \rightarrow \text{3L}$. However, (see Fig. 2) the other two acoustic modes, TA_1 and LA , are coupled to the low - lying optical modes of Ga. Fig. 3 shows how this coupling affects the behaviour of the polarization vectors of Ga for its acoustic modes. The Ga atom type have been chosen for clarity, while acoustic modes of the other atoms show similar trends. Figure 3 illustrates that the acoustic-optical hybridization (compare with Fig. 2) leads to a number of anomalies, which occur at the corresponding wave vector coordinates $\zeta = 0.3$, $\zeta = 0.43$ and $\zeta = 0.715$. A longitudinal-phonon optical mode can be associated to a charge density wave, which gives a sharp peak in the magnetic susceptibility $\chi(q)$. The crossing at $\zeta = 0.43$ compares well with those for which anomalies are ob-

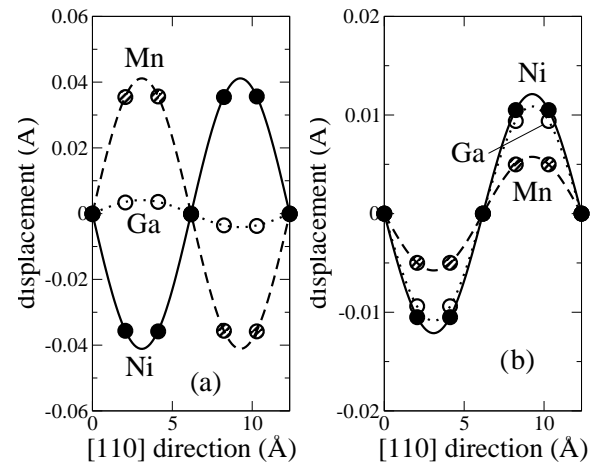


FIG. 4: Displacements of the 3L premartensitic modulated structure: before a) and after b) structural relaxation. The atoms are displaced parallel to a_{orth} in successive $(010)_{\text{orth}}$ planes. The displacements are in a different scale in order to be observed.

served in the susceptibility calculations, which have been associated with the lattice instabilities in the 5L and 7L structures [29, 30]. These crossings correlate in a natural way with the change of the C_{44} elastic constant, which is, as it turns out, not related to the TA_2 branch through the premartensitic transformation. It comes as a novelty that the involvement of the optical modes is required in order to understand the phase transformations in these alloys.

It is interesting to note that the anomaly in the TA_2 branch has been found around the soft mode $[1/3, 1/3, 0](2\pi/a)$ in our calculations, which is the wave vector associated with the phonon anomaly of the premartensitic transition [13]. Also the phonon branches on the [110] direction for the T structure are given in Fig. 2(b). In this latter case, the branches TA_2 and TA_1 become similar and the softening of the TA_2 branch, present in the cubic phase, disappears. This finding is consistent with the stability of the T structure [31] and adds insight into interpreting the experiments [19]. The sequence of the optical modes is different in this case and they are not degenerate at the Γ and X points. The instability of the cubic structure at zero temperature is the clue to understand how the martensite phase may nucleate. Instead of twinnings and stacking faults, the modulation of the martensitic tetragonal structure of Ni_2MnGa corresponds to a smaller structural change easier to accommodate or to derive from the parent cubic structure. With respect to the electronic structure, the lowering of the symmetry allows for a splitting of the density of states peak at the Fermi level [10, 31], thereby decreasing the valence band energy contribution to the total energy. Thus, structural modulation and lowering of the elec-

tronic energy explains the 5L structure of Ni₂MnGa [32].

On the other hand, the recent susceptibility calculations [29, 30] have shown that the peak in the generalized susceptibility at $\mathbf{q} = [\zeta, \zeta, 0](2\pi/a)$ for $\zeta = 0.33$ corresponds to a magnetization of about 60%. This susceptibility peak moves toward higher values of ζ as the magnetization increases: full magnetization leads to a peak at $\zeta = 0.4$. However our calculations show no need for the extra magnetization hypothesis, since all the interesting \mathbf{q} vectors are already present. This casts serious doubts on the role of magnetization in these intermediate or premartensitic transitions. Secondly, this finding reinforces the arguments that the elastic entropy term drives the transition [33] and the spin spirals do not show anomalies involved in the shuffling of the L2₁ structure [34]. In view of these results, the intermediate and the martensitic transition seem to be really independent, although, of course, the L2₁ structure is necessary in order to have the intermediate transformation at $\zeta = 0.33$.

In summary, we have calculated the phonon dispersion for two structures of Ni₂MnGa: the cubic L2₁ and the tetragonal T at zero temperature. The cubic structure is found to be unstable with respect to a specific re-arrangement (shuffling) of the atoms which leads to a modulated super-structure 3L. We have calculated stability of the 3L structure with high accuracy and found that it reflects perfectly our phonon calculations. Furthermore, we have shown that the subtle competition of low-lying optical modes of Ni and acoustic modes account for the experimentally observed wave vectors, for which anomalies have been observed (3L, 5L and 7L structures). These calculations have been done by using first-principles methods, and are in very good agreement with experimental findings.

This work has been supported by the Graduate School "Structure and Dynamics of Heterogeneous Systems" of the Deutsche Forschungsgemeinschaft (DFG) and by the Academy of Finland through its Centers of Excellence Program (2000-2005). Computer facilities of the Research Centre Jülich (Project "Lattice dynamics") are acknowledged. We thank Prof. M. Acet, Prof. K. Parlinski, Dr. A. Postnikov and Prof. A. Planes for valuable discussions.

5774 (2000).

- [5] O. Heczko, A. Sozinov, and K. Ullakko, IEEE Trans. Mag., **36**, 3266 (2000); O. Heczko, K. Jurek, and K. Ullakko, J. Magn. Magn. Mater. **226**, 996 (2001).
- [6] K. Ullakko, J. K. Huang, C. Kantner, R. C. O'Hanley, and V. V. Kokorin, Appl. Phys. Lett. **69**, 1966 (1996).
- [7] I. Aaltio and K. Ullakko, Actuator 2000. Ed.: H. Borgmann. Bremen: Messe Bremen GmbH, 2000.
- [8] A. N. Lavrov, Seiki Komiya, and Yoichi Ando, Nature **418**, 385 (2002).
- [9] R. J. Gooding and J. A. Krumhansl, Phys. Rev. B **39**, 1535 (1989).
- [10] P. J. Brown, J. Crangle, T. Kanomata, M. Matsumoto, K-U. Neumann, B. Ouladdiaf, and K. R. A. Ziebeck, J. Phys.: Condens. Matter **14**, 10159 (2002).
- [11] V. V. Martynov and V. V. Kokorin, J. Physique III **2**, 739 (1992).
- [12] A. Zheludev, S.M. Shapiro, P. Wochner, A. Schwartz, M. Wall, and L.E. Tanner, Phys. Rev. B **51**, 11310 (1995).
- [13] A. Zheludev, S. M. Shapiro, P. Wochner, and L. E. Tanner, Phys. Rev. B **54**, 15045 (1996).
- [14] U. Stuhr, P. Vorderwisch, V.V. Kokorin, and P.-A. Lindgård, Phys. Rev. B **56**, 14360 (1997).
- [15] G. Fritsch, V. V. Kokorin, and A. Kempf, J. Phys.: Condens. Matter **6**, L107 (1994).
- [16] E. Cesari, V. A. Chernenko, V. V. Kokorin, J. Pons, and C. Segu, Acta Mater. **45**, 999 (1997).
- [17] J. Worgull, E. Petti, and J. Trivisonno, Phys. Rev. B **54**, 15695 (1996).
- [18] L. Mañosa, A. González-Comas, E. Obradó, A. Planes, V. A. Chernenko, V. V. Kokorin, and E. Cesari, Phys. Rev. B **55**, 11068 (1997).
- [19] L. Mañosa, A. Planes, J. Zarestky, T. Lograsso, D.L. Schlagel and C. Stassis, Phys. Rev. B **64**, 024305 (2001).
- [20] A. Planes, E. Obradó, A. González-Comas, and L. Mañosa, Phys. Rev. Lett. **79**, 3926 (1997).
- [21] K. Parlinski, Z.-Q. Li, and Y. Kawazoe Phys. Rev. Lett. **78**, 4063 (1997).
- [22] K. Parlinski, *PHONON software manual, version 3.11*, Cracow, Poland (2002).
- [23] G. Kresse and J. Furthmüller, Phys. Rev. B **54**, 11169 (1996).
- [24] G. Kresse and D. Joubert, Phys. Rev. B **59**, 1758 (1999).
- [25] P. E. Blöchl, Phys. Rev. B **50**, 17953 (1994).
- [26] J. Enkovaara, A. Ayuela, and R.M. Nieminen (in preparation).
- [27] The plane-wave cutoff energy of 353.4 eV and the Monkhorst-Pack k-point generation scheme is used with a grid of $10 \times 8 \times 2$ points in the full Brillouin zone.
- [28] The k-point sampling is now $13 \times 6 \times 18$.
- [29] O. I. Velikokhatni and I. I. Naumov, Phys. Solid State **41**, 617 (1999).
- [30] Y. Lee, J. Y. Rhee, and B. N. Harmon, Phys. Rev. B **66**, 054424 (2002).
- [31] A. Ayuela, J. Enkovaara, K. Ullakko, and R. M. Nieminen, J. Phys.: Condens. Matter **11**, 2017 (1999); A. Ayuela, J. Enkovaara, and R.M. Nieminen, J. Phys.: Condens. Matter **14**, 5325 (2002).
- [32] A. T. Zayak, P. Entel, J. Enkovaara, A. Ayuela, and R. M. Nieminen, J. Phys.: Condens. Matter **15**, 159 (2003).
- [33] J. Enkovaara, A. Ayuela, L. Nordström, and R.M. Nieminen, J. Appl. Phys. **91**, 7798 (2002).
- [34] J. Enkovaara, A. Ayuela, J. Jalkanen, L. Nordström, R.M. Nieminen, Phys. Rev. B. **67**, 054417 (2003).

- [1] P. J. Webster, K. R. A. Ziebeck, S. L. Town, and M. S. Peak, Philos. Mag. A **49**, 295 (1984).
- [2] I. Takeuchi, O. O. Famodu, J. C. Read, M. A. Aronova, K.-S. Chang, C. Craciunescu, S. E. Lofland, M. Wuttig, F. C. Wellstood, L. Knauss and A. Orozco, Nature Materials **2**, 180 (2003).
- [3] K. Ullakko, A. Sozinov, and P. Yakovenko, cond-mat/0004211.
- [4] S. J. Murray, M. A. Marioni, A. M. Kukla, J. Robinson, R. C. O'Hanley, and S. M. Allen, J. Appl. Phys. **87**,